Journal of Alloys and Compounds 509 (2011) 3132–3135

Contents lists available at ScienceDirect

Journal of Alloys and Compounds

journal homepage: www.elsevier.com/locate/jallcom

Formation mechanisms of ZnO nanocrystals embedded in an amorphous $Zn_{2x}Si_{1-x}O_2$ layer due to sputtering and annealing

J.W. Shin[a,d], J.Y. Lee[a], Y.S. No[b], T.W. Kim[b,*], W.K. Choi[c]

[a] Department of Materials Science and Engineering, KAIST, Daejeon 305-701, Republic of Korea
[b] National Research Laboratory for Nano Quantum Electronics, Department of Electronics and Computer Engineering, Hanyang University, 17 Haengdang-dong, Seongdong-gu, Seoul 133-791, Republic of Korea
[c] Thin Film Material Research Center, Korea Institute of Science and Technology, Seoul 136-701, Republic of Korea
[d] Division of Electron Microscopic Research, Korea Basic Science Institute (KBSI), 113 Gwahangno, Yuseong-gu, Daejeon 305-333, Republic of Korea

ARTICLE INFO

Article history:
Received 20 July 2010
Received in revised form 1 December 2010
Accepted 3 December 2010
Available online 10 December 2010

PACS:
68.37.Lp
68.65.Hb

Keywords:
Oxide materials
Semiconductors
Surfaces and interfaces
Thin films
Atomic scale structure
Transmission electron microscopy
TEM

ABSTRACT

ZnO nanocrystals embedded in an amorphous $Zn_{2x}Si_{1-x}O_2$ layer inserted between a ZnO thin film and a p-Si (1 0 0) substrate were formed by magnetron sputtering and thermal annealing. High-resolution transmission electron microscopy (HRTEM) images showed that ZnO nanocrystals were embedded in the $Zn_{2x}Si_{1-x}O_2$ layer inserted into a ZnO/Si heterostructure. The $\{0\,1\,\bar{1}\,0\}$ planes were observed for the ZnO nanocrystals with a [0 0 0 1] orientation direction, and the $\{0\,1\,\bar{1}\,1\}$ and the {0 0 0 1} planes were observed for the ZnO nanocrystal with a $[2\,\bar{1}\,\bar{1}\,0]$ orientation direction. The formation of ZnO nanocrystals consisting of the most stable {0 0 0 1} and $\{0\,1\,\bar{1}\,1\}$ facet planes was attributed to atomic rearrangement of Zn and O atoms to reduce the surface energy during the thermal annealing and the cooling processes. The formation mechanisms for the ZnO nanocrystals embedded in an amorphous $Zn_{2x}Si_{1-x}O_2$ layer inserted into a ZnO/p-Si (1 0 0) heterostructure were described on the basis of the HRTEM images.

1. Introduction

Since ZnO compounds are wide band-gap semiconductors with unique physical properties of large exciton binding energies and large direct band gap [1–3], they are of current interest due to their potential applications in optoelectronic devices, such as solar cells [4,5], light-emitting diodes [6,7] and laser diodes [8]. The formation and the physical properties of dimensional structures of ZnO quantum dots, ZnO nanowires, ZnO-based quantum wells, and ZnO thin films have received much attention due to current tendency to fabricate optoelectronic devices operating in the ultraviolet (UV) region of the spectrum due to their wider band gap [9–13]. Among the various dimensional structures of the ZnO materials, ZnO nanocrystals have been particularly attractive because of their promising applications in next-generation optoelectronic devices, such as UV photodetectors [14,15]. Even though some studies concerning the formation of ZnO nanocrystals have been conducted [16–22], very few studies on the fabrication of ZnO nanocrystals by using simple methods, such as sputtering and thermal annealing, have been performed [21,22]. Furthermore, studies on the formation mechanisms of ZnO nanocrystals embedded in an insulator layer have emerged as potential candidates for promising applications in next-generation memory devices [23].

This paper reports data for the formation mechanisms of ZnO nanocrystals embedded in an amorphous $Zn_{2x}Si_{1-x}O_2$ layer inserted into a ZnO/p-Si (1 0 0) heterostructure by using sputtering and thermal annealing. Transmission electron microscopy (TEM) measurements were carried out in order to investigate the microstructures and morphologies of the ZnO nanocrystals embedded in the ZnO/Si heterostructures. The formation mechanisms for the ZnO nanocrystals embedded in an amorphous $Zn_{2x}Si_{1-x}O_2$ layer inserted into a ZnO/p-Si (1 0 0) heterostructure are described on the basis of the experimental results.

2. Experimental details

Polycrystalline stoichiometric ZnO with a purity of 99.999% was used as a source for the RF sputter target material and was precleaned by repeated sublimation. The carrier concentration of the B-doped p-Si substrates with (1 0 0) orientations

* Corresponding author. Tel.: +82 2 2220 0354; fax: +82 2 2292 4135.
E-mail address: twk@hanyang.ac.kr (T.W. Kim).

0925-8388/$ – see front matter © 2010 Elsevier B.V. All rights reserved.
doi:10.1016/j.jallcom.2010.12.021

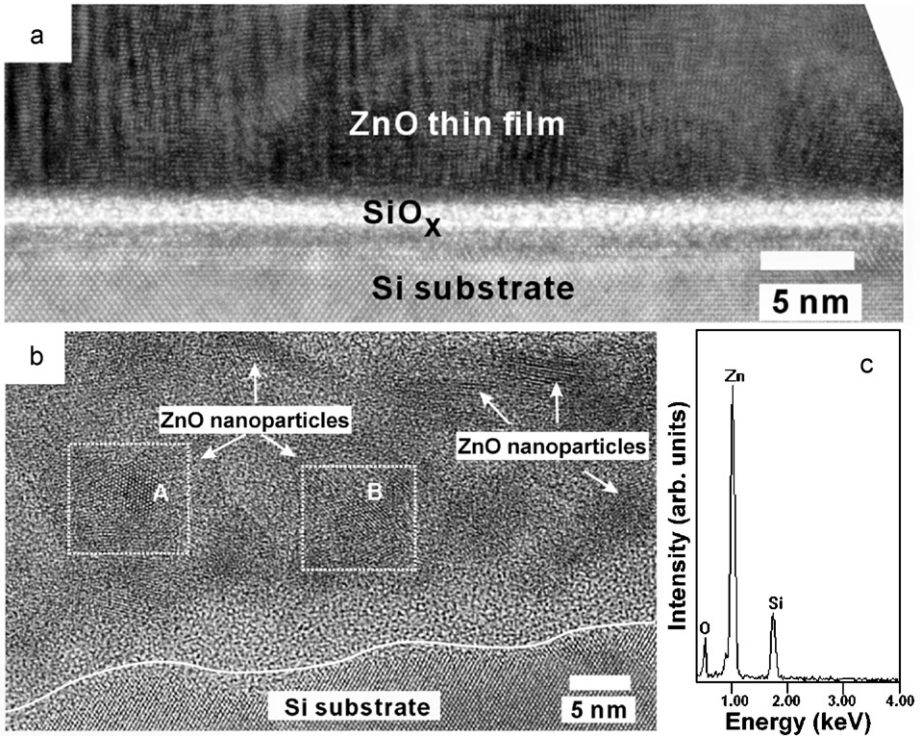

Fig. 1. High-resolution transmission electron microscopy images of the (a) as-grown and the (b) annealed ZnO thin films grown on p-Si (1 0 0) substrates and (c) energy dispersive spectroscopy spectrum for the amorphous intermediate layer shown in (b).

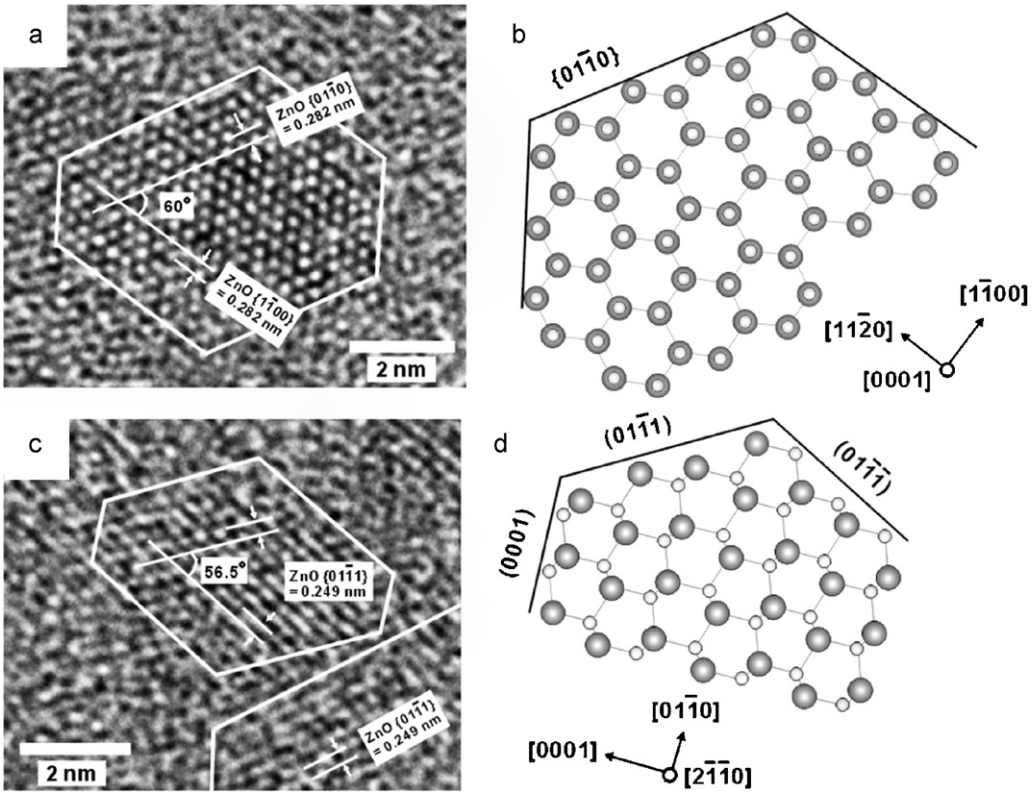

Fig. 2. High-resolution transmission electron microscopy images of crystalline ZnO nanocrystals oriented with (a) [0 0 0 1] and (c) [2 $\bar{1}$ $\bar{1}$ 0] directions parallel to the incident electron beam, respectively. These are highly magnified images of the A and the B regions corresponding to the crystalline ZnO nanocrystals in Fig. 1(b). (b) and (d) are the corresponding schematic diagrams of the atomic arrangements of the A and the B regions corresponding to the crystalline ZnO nanocrystals, respectively. The smaller and the larger circles denote Zn and O, respectively.

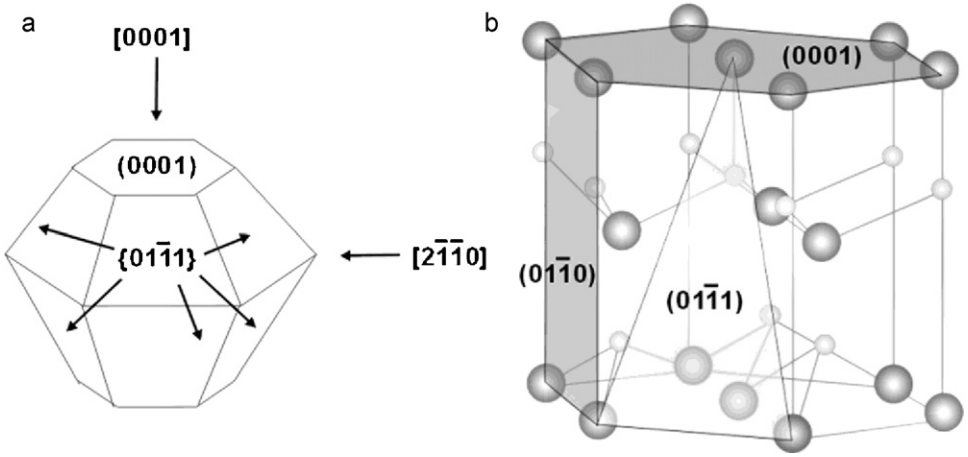

Fig. 3. (a) Possible three-dimensional structure of a crystalline ZnO nanocrystals embedded in an amorphous layer inserted between the ZnO thin film and the Si substrate. (b) Schematic diagram of the crystal structure of ZnO showing lower surface energy planes. The smaller and the larger circles denote Zn and O, respectively.

used in this experiment was 1×10^{15} cm^{-3}. The Si substrates were degreased in trichloroethylene (TCE), rinsed in de-ionized water, etched in a mixture of acetone, methanol, and ethanol by using ultrasonications, and rinsed in TCE again. After the Si substrates had been chemically cleaned, they were mounted onto a susceptor in a growth chamber. Argon gas with a purity of 99.999% was used as the sputtering gas [24]. The distance between the plasma gun and the substrate was 6 cm. Prior to the ZnO growth, the surface of the ZnO target was cleaned by Ar^+ sputtering. After the chamber had been evacuated to 1×10^{-7} Torr, the RF sputter deposition of the ZnO film (frequency = 13.26 MHz, power = 100 W) was carried out at a system pressure of 1.2×10^{-2} Torr and a substrate temperature of 250 °C. The gas flow-rate ratio of Ar to O_2 was 1, and the ZnO film growth rate was approximately 13 nm/min. The thickness of the ZnO thin film was approximately 100 nm. The thermal annealing process was performed in a nitrogen atmosphere with a tungsten–halogen lamp as the thermal source. The thermal annealing process was carried out for 20 min at 900 °C.

The TEM measurements were performed using a Tecnai F30 S-twin transmission electron microscope operating at 300 keV [25]. The samples for the cross-sectional TEM measurements were prepared by cutting and polishing them to a thickness of approximately 30 μm and then argon-ion milling at liquid-nitrogen temperature to electron transparency.

3. Results and discussion

Fig. 1 shows the high-resolution TEM (HRTEM) images of the (a) as-grown and the (b) annealed ZnO thin films grown on p-Si (1 0 0) substrates. When the ZnO thin film was grown on the p-Si (1 0 0) substrate by using the sputtering method, an amorphous SiO_x thin layer was formed, resulting from the reaction of oxygen ions with the Si surface during the sputtering process. When the ZnO thin film grown on the p-Si (1 0 0) substrate was annealed at 900 °C, an amorphous $Zn_{2x}Si_{1-x}O_2$ layer was formed between the ZnO thin film and the Si substrate. The compositional characteristics of the ZnO/Si heterointerface region after 900 °C were investigated by using energy dispersive spectroscopy (EDS) measurements, as shown in Fig. 1(c). While the crystal ZnO and Si lattice images at the just beside of the interface layer are clearly observed, the lattice fringes do not appear at the interface layer, indicative of the amorphous phase of the interface layer. The EDS spectrum demonstrated that the formed layer at the ZnO/Si heterointerface region consisted of Zn, Si, and O atoms, indicative of the formation of the $Zn_{2x}Si_{1-x}O_2$ layer. The formation of the amorphous $Zn_{2x}Si_{1-x}O_2$ layer was attributed to an interdiffusion of Zn, O, and Si atoms existing in the heterointerface region due to thermal treatment, resulting in the concomitant increase in the thickness of the amorphous interface layer [25,26]. The crystalline ZnO nanocrystals with sizes of 5–8 nm were embedded in the amorphous oxide layer, as determined from the HRTEM images shown in Fig. 2. The formation of ZnO nanocrystals embedded in the amorphous layer is attributed to atomic rearrangements of Zn and O atoms in the amorphous $Zn_{2x}Si_{1-x}O_2$ layer during the thermal annealing and the cooling processes.

Fig. 2(a) and (c) shows HRTEM images of crystalline ZnO nanocrystals oriented with [0 0 0 1] and [2 $\bar{1}$ $\bar{1}$ 0] directions parallel to the incident electron beam, respectively. These are highly magnified images of the A and the B regions corresponding to the ZnO nanocrystals in Fig. 1(b). The corresponding schematic diagrams of the atomic arrangement of the A and the B regions corresponding to the crystalline ZnO nanocrystals are shown in Fig. 2(b) and (d), respectively. The smaller and the larger circles shown in Fig. 2(b) and (d) denote Zn and O, respectively. The interplanar spacing distance of the {0 1 $\bar{1}$ 0} planes and the angle of the plane for the region A corresponding to the crystalline ZnO nanocrystals are 0.282 nm and 60°, respectively, and the interplanar spacing distance of the {0 1 $\bar{1}$ 1} planes and the angle of the plane for the region B corresponding to the ZnO nanocrystals are 0.249 nm and 56.5°, respectively [27,28]. The interplanar spacing distances of the ZnO nanocrystal are in reasonable agreement with those of the ZnO bulk.

A possible three-dimensional structure of the ZnO nanocrystals embedded in the amorphous layer inserted between the ZnO thin film and the Si substrate can be suggested on the basis of the HRTEM results. The {0 1 $\bar{1}$ 0} planes are observed for the ZnO nanocrystals with a [0 0 0 1] orientation direction, and the {0 1 $\bar{1}$ 1} and the {0 0 0 1} planes are observed for the ZnO nanocrystal with a [2 $\bar{1}$ $\bar{1}$ 0] orientation direction, as shown in Fig. 2. Thus, the three-dimensional structure of a ZnO nanocrystal is composed of {0 0 0 1} and {0 1 $\bar{1}$ 1} planes with a spherical shape, as shown in Fig. 3(a). Because the two lowest surface energy planes, {0 0 0 1} and {0 1 $\bar{1}$ 1} planes, exist in the ZnO crystal [29], ZnO nanocrystals, which are composed of the most stable facets with {0 0 0 1} and {0 1 $\bar{1}$ 1} planes, might be created to reduce the surface energy during the thermal annealing and the cooling processes. Fig. 3(b) shows a schematic diagram of the crystal structure of ZnO showing lower surface energy planes, which are composed of {0 0 0 1} and {0 1 $\bar{1}$ 1} planes. The smaller and the larger circles shown in Fig. 3(b) denote Zn and O, respectively.

When the ZnO thin film is grown on the p-Si (1 0 0) substrate by using the sputtering method, an amorphous SiO_x thin layer with a thickness of approximately 3 nm is formed between the ZnO thin film and the Si substrate, as shown in Fig. 1(a). The formation of this amorphous layer might be attributed to a reaction between oxygen and the Si substrate during ZnO deposition. When the ZnO thin film grown on the p-Si (1 0 0) substrate is annealed at 900 °C, an amorphous $Zn_{2x}Si_{1-x}O_2$ layer is formed between the ZnO thin film and the Si substrate due to a reaction among Zn, Si and oxygen. The formation of crystalline ZnO nanocrystals, which are composed of

the most stable facets with {0 0 0 1} and {0 1 $\bar{1}$ 1} planes, embedded in the amorphous layer, is attributed to an atomic rearrangement of Zn and O atoms in the amorphous $Zn_{2x}Si_{1-x}O_2$ layer during the thermal annealing and the cooling processes.

4. Summary and conclusions

ZnO nanocrystals embedded in an amorphous $Zn_{2x}Si_{1-x}O_2$ layer inserted into ZnO/p-Si (1 0 0) heterostructures were formed by using the magnetron sputtering and thermal annealing. HRTEM images showed that ZnO nanocrystals with sizes between 5 and 8 nm were embedded in the amorphous $Zn_{2x}Si_{1-x}O_2$ layer. The formation of ZnO nanocrystals composed of the most stable {0 0 0 1} and {0 1 $\bar{1}$ 1} facet planes was related to atomic rearrangement of Zn and O atoms that reduce the surface energy during the thermal annealing and the cooling processes. The formation mechanisms for the ZnO nanocrystals embedded in an amorphous $Zn_{2x}Si_{1-x}O_2$ layer inserted into a ZnO/p-Si (1 0 0) heterostructure were described on the basis of the HRTEM images. These results can help improve understanding of formation mechanisms of ZnO nanocrystals embedded in an amorphous $Zn_{2x}Si_{1-x}O_2$ layer due to sputtering and annealing.

Acknowledgment

This work was supported by the National Research Foundation of Korea (NRF) grant funded by the Korea government (MEST) (No. 2010-0018877).

References

[1] M.H. Huang, S. Mao, H. Feick, H.Q. Yan, Y.Y. Wu, H. Kind, E. Weber, R. Russo, P.D. Yang, Science 292 (2001) 1897–1899.
[2] T. Makino, Y. Segawa, A. Tsukazaki, A. Ohtomo, M. Kawasaki, Appl. Phys. Lett. 87 (2005), 022101-1–122101-3.
[3] Y.H. Tong, Y.C. Liu, C.L. Shao, R.X. Mu, Appl. Phys. Lett. 88 (2006), 123111-1–1123111-3.
[4] B. Postels, A. Kasprzak, T. Buergel, A. Bakin, E. Schlenker, H.H. Wehmann, A. Waag, J. Kor. Phys. Soc. 53 (2008) 115–118.
[5] U. Rau, M. Schmidt, Thin Solid Films 387 (2001) 141–146.
[6] S. Gangil, A. Nakamura, K. Yamamoto, T. Ohashi, J. Temmyo, J. Kor. Phys. Soc. 53 (2008) 212–217.
[7] W.Z. Xu, Z.Z. Ye, Y.J. Zeng, L.P. Zhu, B.H. Zhao, L. Jiang, J.G. Lu, H.P. He, Appl. Phys. Lett. 88 (2006), 173506-1–1173506-3.
[8] H. Kim, C.M. Gilmore, J.S. Jorwitz, A. Pigue, H. Murafa, G.P. Kushto, R. Schlaf, Z.H. Kafafi, D.B. Chrisey, Appl. Phys. Lett. 76 (2000) 259–261.
[9] A. Tsukazaki, A. Ohtomo, T. Onuma, M. Ohtani, T. Makino, M. Sumiya, K. Ohtani, S.F. Chichibu, S. Fuke, Y. Segawa, H. Ohno, H. Koinuma, M. Kawasaki, Nat. Mater. 4 (2005) 42–46.
[10] K.C. Hui, H.C. Ong, P.F. Lee, J.Y. Dai, Appl. Phys. Lett. 86 (2005), 152116-1–1152116-3.
[11] F.X. Xiu, L.J. Mandalapu, Z. Yang, J.L. Liu, G.F. Liu, J.A. Yarmoff, Appl. Phys. Lett. 89 (2006), 052103-1–152103-3.
[12] J.W. Shin, J.Y. Lee, Y.S. No, T.W. Kim, W.K. Choi, Appl. Phys. Lett. 89 (2006), 101904-1–101904-3.
[13] M.A. Garcia, J.M. Merino, E.F. Pinel, A. Quesada, J. de la Venta, M.L.R. González, G.R. Castro, P. Crespo, J. Llopis, J.M. González-Calbet, A. Hernando, Nano Lett. 7 (2007) 1489–1494.
[14] H.M.P. Wong, P. Wang, A. Abrusci, M. Svensson, M.R. Andersson, N.C. Greenham, J. Phys. Chem. C 111 (2007) 5244–5249.
[15] Y. Jin, J. Wang, B. Sun, J.C. Blakesley, N.C. Greenham, Nano Lett. 8 (2008) 1649–1653.
[16] Y.F. Guan, A.J. Pedraza, Nanotechnology 19 (2008), 045609-1–145609-7.
[17] S. Bhattacharya, A. Ghosh, Appl. Phys. Lett. 88 (2006), 133122-1–1133122-7.
[18] P. Lommens, D.V. Thourhout, P.F. Smet, D. Poelman, Z. Hens, Nanotechnology 19 (2008), 245301-1–1245301-6.
[19] F. Li, T.W. Kim, W. Dong, Y.H. Kim, Appl. Phys. Lett. 92 (2008), 011906-1–111906-3.
[20] T. Tsuzukia, P.G. McCormick, Scr. Mater. 44 (2001) 1731–1734.
[21] K.K. Kim, N. Koguchi, Y.W. Ok, T.Y. Seong, S.J. Park, Appl. Phys. Lett. 84 (2004) 3810–3812.
[22] S.W.H. Eijt, J. de Roode, H. Schut, B.J. Kooi, J.T.M. De Hosson, Appl. Phys. Lett. 91 (2007), 201906-1–1201906-3.
[23] K.H. Park, J.H. Jung, F. Li, D.I. Son, T.W. Kim, Appl. Phys. Lett. 93 (2008), 132104-1–1132104-3.
[24] J.W. Shin, J.Y. Lee, Y.S. No, T.W. Kim, W.K. Choi, Appl. Phys. Lett. 89 (2006), 101904-1–1101904-3.
[25] J.W. Shin, J.Y. Lee, Y.S. No, T.W. Kim, W.K. Choi, S. Jin, Nanotechnology 19 (2008), 295303-1–1295303-6.
[26] T.W. Kim, J.W. Shin, J.Y. Lee, J.H. Jung, J.W. Lee, W.K. Choi, S. Jin, Appl. Phys. Lett. 90 (2007), 051915-1–151915-3.
[27] D.B. Williams, C.B. Carter, Transmission Electron Microscopy, vol. 3, Plenum Press, 1996, pp. 271–273.
[28] S.C. Abrahams, J.L. Bernstein, Acta Crystallogr. B 25 (1969) 1233–1236.
[29] J. Zuniga-Perez, V. Munoz-Sanjose, E. Palacios-Lidon, J. Colchero, Appl. Phys. Lett. 88 (2006), 261912-1–1261912-3.